Rotational energy transfer in collisions between CO and Ar at temperatures from 293 to 30 K

Laura A. Mertens,[a,b] Hamza Labiad,[a] Otoniel Denis-Alpizar,[c, d] Martin Fournier,[a] David Carty,[e] Sébastien D. Le Picard,[a] Thierry Stoecklin[c] and Ian R. Sims[a]*

[a]Institut de Physique de Rennes, Département Physique Moléculaire, UMR 6251 du CNRS - Université de Rennes 1, 263 Avenue du Général Leclerc, 35042 Rennes Cedex, France

[b]Division of Chemistry and Chemical Engineering, California Institute of Technology, Pasadena, California 91125, United States

[c]Institut des Sciences Moléculaires, Université de Bordeaux, CNRS-UMR 5255, 33405 Talence, France

[d]Instituto de Ciencias Químicas Aplicadas, Universidad Autónoma de Chile. El Llano Subercaseaux 2801, San Miguel, Santiago, Chile.

[e]Durham University, Joint Quantum Centre Durham-Newcastle, Departments of Physics and Chemistry, Lower Mountjoy, South Road, Durham, UK, DH1 3LE

Abstract

Experimental measurements and theoretical calculations are reported for rotational energy transfer in the Ar-CO system. Experiments were performed in cold uniform supersonic flows of Ar, using an infrared – vacuum ultraviolet double resonance technique to measure absolute state-to-state rate constants and total relaxation cross sections for rotational energy transfer within the (v = 2) vibrational state of CO in collision with Ar at temperatures from 30.5 to 293 K. Close-coupled calculations were also performed using a recent potential energy surface (Y. Sumiyoshi and Y. Endo, J. Chem. Phys. 142 (2015) 024314). Excellent agreement is obtained between measured and calculated values.

1. Introduction

Ar-CO is a model system for understanding intermolecular forces [1] as, owing to its large polarizability, van der Waals forces are stronger for Ar than for smaller atoms, such as He. Understanding these long-range forces is essential to calculating many properties of gases [1-4]. A reliable potential energy surface describing these intermolecular forces can be used to calculate bulk properties of gases including viscosity, diffusion, thermal conductivity, and virial coefficients [5-9]. These long-range forces also influence pressure broadening of spectra; larger van der Waals forces generally lead to more broadening. So, an understanding of long-range forces is needed to predict accurately the spectra of atoms and molecules [3,4,10-12]. Intermolecular forces control the rates of barrierless gas-phase chemical reactions at low temperatures [13-15], as well as collisional rotational energy transfer (RET) in gases [16].

Rate constants for RET are needed to understand many gas-phase phenomena, including the propagation, absorption and dispersion of sound waves and the transport properties of gases. They are also needed to predict the lifetimes of energetically excited molecules – these "hot" molecules can react differently leading to new product channels or non-thermal product distributions [17]. RET, particularly at low temperatures, is of great importance in deriving column densities in the interstellar medium [18,19].

While theoretical methods can provide extensive matrices of state-to-state rate constants for RET, the accuracy of these calculations, especially at low temperatures, depends on the quality of the available potential energy surfaces. Simple systems such as CO – Ar [1] provide an opportunity to benchmark theoretical calculations and improve their predictive power. Noble gas – diatomic molecule complexes represent the simplest systems where anisotropic intermolecular forces play an important role. The Ar – CO complex represents a theoretical challenge as the potential, and particularly its anisotropic part, is largely determined by the balance between dispersion and repulsion. The accurate calculation of the dispersion interaction, including correlation effects, is particularly challenging.

A number of potential energy surfaces for Ar-CO have been published [1,20-24], and used to predict results to compare with a variety of experiments, including studies on the collisional line broadening of CO in Ar [10-12,25,26] and spectroscopic studies of the Ar-CO van der Waals complex [27-30]. Havenith and Schwaab summarized many of these studies in their 2005 review article [1]. Recently, Sumiyoshi and Endo [20] have provided an updated survey and a high quality 3D potential energy surface for the Ar-CO system from *ab initio* coupled cluster calculations at the CCSD(T)-F12b/aug-cc-pV5Z level of theory. They parameterized this potential energy surface and performed optimization using spectroscopic data on the Ar-CO complex. State-to-state rate constants for RET would provide an additional test of this potential energy surface, especially at low temperatures where the collision energy is of the same order or less than the Ar-CO van der Waals well depth. Low temperature RET

measurements are particularly sensitive to the hard-to-determine long-range anisotropic part of the potential. While state-to-state rate constants for RET have been reported for CO in He, much less has been published on rates of RET between CO and Ar [31-33]. In 1999, Belikov and Smith [33] measured rotational relaxation rate constants for CO in Ar supersonic expansions by electron beam fluorescence and REMPI techniques at 7—150 K. However, they did not perform these measurements under uniform temperature conditions and instead determined rate constants by fitting populations and line widths in the evolving free jet expansions to various pre-determined fitting laws.

Here, we report direct measurements of total and state-to-state rate constants for RET of CO in Ar between 30 and 295 K using infrared-vacuum ultraviolet double resonance (IRVUVDR) in cold uniform supersonic flows in a CRESU (Cinétique de Réaction en Ecoulement Supersonique Uniforme or Reaction Kinetics in a Uniform Supersonic Flow) apparatus. The results are compared to close-coupled quantum scattering calculations performed on the recently published PES of Sumiyoshi and Endo [20].

2. Experimental and Theoretical Methods

2.1. Experimental apparatus and techniques

The CRESU technique was first developed by Rowe and co-workers [34,35] for the study of ion-molecule reaction kinetics, and has subsequently been adapted for investigations of both neutral-neutral kinetics [36] and energy transfer at temperatures as low as 7 K [18,37-39]. The CRESU and IRVUVDR techniques have been described in detail in James *et al*. [39] and Carty *et al.* [18]. VUV laser induced fluorescence (LIF) provides a sensitive detection method, allowing us to work with very low [CO] (<0.5%). The pulsed lasers used in this study have a time resolution of ca. 5 ns, enough to probe the fast kinetics of RET under the conditions prevailing in the cold supersonic flows.

CO molecules are excited to their initially unpopulated second (v = 2) vibrationally excited state by an infrared pulse that counter-propagates along the axis of the supersonic expansion. By tuning the frequency of the IR laser, the initial rotational level in the excited vibrational state may be chosen. Through collisions with the Ar bath gas, the vibrationally excited CO molecules will relax to rotational equilibrium (vibrational relaxation is observed to be negligible on the timescales, 0 – 2 μs, of the experiments), and at any time the rotational state populations of the CO can be probed by LIF in the $A^1\Pi - X^1\Sigma^+$ (0,2) VUV band of CO.

IR light was produced by a LaserVision KTP combined optical parametric oscillator (OPO) – optical parametric amplifier (OPA), pumped by a Continuum Surelite EX injection-seeded Nd:YAG laser operated at 10 Hz. 5-10 mJ IR pulses were produced at 2349.5, 2351.67, 2358.41, or 2363.12 nm to study J = 0, 1, 4 and 6, respectively. Strong fluctuations in IR pulse

energy (between 5 and 10 mJ) were observed as well as frequency fluctuations of 0.04 nm (2σ standard deviation). To reduce noise from these fluctuations, we discriminated data points based upon signal received from a custom-built photoacoustic cell filled with 8 mbar of CO [18]. The photoacoustic signal from this cell was amplified with a Stanford Research SR560 low-noise voltage amplifier before being integrated with a Stanford Research SR250 gated integrator with a 15 μs gate. Data points were discarded for which the photoacoustic signal was below a predetermined threshold (generally set at ~1.2 times the average photoacoustic signal).

VUV light needed for LIF detection of the vibrationally excited CO was produced through 4-wave difference frequency mixing in Xe gas as described by Hilbig and Wallenstein [40] and employed in Carty *et al*. [18]. In this method, VUV light is produced using two 256.01 nm photons to excite the $5p^5 6p(5/2)_2 \leftarrow 5p^6\ ^1S_0$ transition of Xe. A visible photon at 565.5 – 567.5 nm stimulates the emission of photons at 565.5 – 567.5 nm and 165.29 – 165.45 nm. The 256.01 nm light is produced with a Sirah Lasertechnik Cobra-Stretch dye laser with Coumarin 503 dye (Exciton) pumped by a frequency tripled Continuum Precision II Nd:YAG laser (355 nm) operated at 10 Hz. The output of the dye laser (512.02 nm) was frequency doubled with a BBO crystal to produce ~1 mJ of the desired 256.01 nm light. The frequency doubled output of the Nd:YAG laser (532 nm) also pumped a Laser Analytical Systems LDL 20505 dye laser operated with Rhodamine 6G dye (Exciton) dye to produce ~8 mJ/pulse of 565.5 – 567.5 nm light. These two beams were focused by an 18 cm (at 256 nm) focal length lens through a fused silica window into a cell filled with 2.7 mbar of Xe. In addition the visible light was pre-focused through a 150 cm (at 565 nm) focal length lens. The VUV light produced was re-collimated by a 10.4 cm (at 166 nm) focal length MgF_2 lens (Crystran Ltd) into the CRESU chamber perpendicular to the IR beam.

The resulting LIF was detected by a solar blind photomultiplier (ET Enterprises 9403B) equipped with a bandpass interference filter (Acton Research) centered at 158.9 nm with a 23.4 nm bandwidth. The signal from the photomultiplier was sent to a gated integrator (Stanford Research SR250) where the signal was integrated with a 16 ns gate and sent to the computer to be recorded. Timing between the IR and the VUV pulses was controlled with two digital delay generators (Stanford Research SR535).

Three different nozzles were used to produce supersonic flows at 110.6 K (with a density of 2.7×10^{16} cm^{-3} and a flow of 44 standard liters per min (SLM) of Ar), 52.2 K (5.2×10^{16} cm^{-3} with a flow of 44 SLM of Ar), and 30.5 K (1.9×10^{16} cm^{-3} with a flow of 15.5 SLM of Ar) in addition to a laminar subsonic flow at room temperature, 293 K ($2 - 4 \times 10^{16}$ cm^{-3} with a flow of 2 - 3 SLM of Ar). The pressures in the chamber and the gas reservoir were measured using absolute capacitance manometers (MKS Baratron), and flows were controlled with mass-flow controllers (MKS 1179A and 1559A). In all experiments the CO concentration was kept at or below 0.6% of the Ar concentration, so we expect minimal interference from CO/CO collisions.

Pressure and temperature in the supersonic expansion were determined by means of impact pressure measurements employing a Pitot probe [36]. All pressures and flows during experiments were within 5% of the conditions for the Pitot measurements. Ar (Air Liquide, 99.995 %) and CO (Air Liquide, 99.998 %) were used directly from their cylinders with no further purification.

2.2. Experimental procedure and data analysis

We performed two types of experiments: a total-removal experiment in which we followed the decay of the initially excited rotational state population with time and state-to-state experiments by which we obtained state-to-state rate constants using spectra at very short delay times. These data analysis methods have been previously discussed in greater detail by Carty *et al*. [18] and James *et al*. [39].

2.2.1. Total Removal Rate Constants and Cross Sections

The frequency of the IR laser selects a rotational state, J_i, in which the entire CO population in $v = 2$ initially resides. Within ~1μs the population relaxes to rotational equilibrium. The total rate for collisional rotational relaxation from a given rotational level (we chose $J_i = 0$, 1, 4, and 6) can be found by recording the decay of the LIF signal of Q(J_i) as a function of time. We chose the Q branch of the $A^1\Pi - X^1\Sigma^+$ (0,2) band of CO because it is more intense than the P branch and its lines are more isolated than the R branch. A typical decay is shown in **Figure 1**. The decays were fit to a simple exponential model with a floating baseline using the Levenberg-Marquardt algorithm to find the first order exponential decay rate constant, $k_{exp,}$ which is the inverse of the exponential decay time, τ. Since there is significant reverse transfer from all of the other states, $J_{f,,}$ to the initial state, J_i, k_{exp}, must be corrected with the following equation in order to find the first order rate constant for total removal from $J_{i,}$, k_{tot}:

$$k_{tot} = \frac{k_{\exp}(1 - f_{J_i}^{eq})}{[\mathrm{Ar}]} \qquad (1)$$

where $f_{J_i}^{eq}$ is the Boltzmann factor of J_i at rotational equilibrium divided by the partition function, or simply the proportion of CO molecules in state J_i at equilibrium. This equation assumes that the rate constant for the reverse reaction at any time is equal to the reverse rate constant from an equilibrium distribution of states. Thus, the kinetics model assumes a simple forward and reverse rate between two states: J_i and a fully rotationally relaxed equilibrium distribution.

The exponential traces do not decay to zero, since J_i will be populated at rotational equilibrium, as illustrated in **Figure 1**. As the baseline is determined by the population in J_i at rotational equilibrium, we can calculate the rotational temperature by dividing the baseline by the fitted LIF intensity at $t = 0$ (which represents the total initial population). All values of rotational

temperatures calculated with this method were found to be within error (2σ) of the temperatures measured by the Pitot probe. The temperatures were also confirmed by the relative intensities of peaks, which always followed a Boltzmann distribution for the expected temperature.

2.2.2. State-to-State Rate Constants

We also determined individual state-to-state rate constants from J_i (again we chose J_i = 0, 1, 4, and 6) to J_f (for J_f = 0 – 10), following the same procedure as in Carty *et al.* [18] recording two LIF DR spectra at different fixed delay times. The first spectrum is recorded at a delay (δt) that is short (15—50 ns) compared with the relaxation time from the selected level in collisions between CO molecules and Ar atoms, so that we can neglect the transfer of molecules in secondary collisions. The observed populations are therefore entirely the result of collisions between CO molecules in the level J_i and Ar atoms. Under these conditions, the rate of population transfer into any collisionally populated level J_f can be described by the equation:

$$dN_{J_f} \Big/ dt = k_{J_i \to J_f} N_{J_i} [\mathrm{Ar}] \qquad (2)$$

which, if δt is sufficiently short, can be written in the approximate form:

$$k_{J_i \to J_f} = \left(\delta N_{J_f} \Big/ N^0_{J_i} \right) \Big/ \delta t [\mathrm{Ar}] \qquad (3)$$

where $N^0_{J_i}$ is the concentration of CO molecules initially excited by the IR pump laser to J_i, and δN_{J_f} is the small concentration found in level J_f at the delay of δt. In this case we chose times sufficiently short compared to the overall relaxation time that this "initial rates" approximation would not result in more than 10% deviation compared to a simple exponential dependence. The concentration of CO in state J_f at time δt can be found from the intensity of J_f LIF for the $A^1\Pi$ – $X^1\Sigma^+$ (0,2) band of CO, $I^{\delta t}_{J_f}$. We also need to correct for the total population of CO that started in J_i, which is given by $I^{eq}_{J_f} \Big/ f^{eq}_{J_f}$ yielding the following equation for the rotational relaxation rate constant from J_i to J_f:

$$k_{J_i \to J_f} = \left(\frac{I^{\delta t}_{J_f} f^{eq}_{J_f}}{I^{eq}_{J_f}} \right) \frac{1}{\delta t [Ar]} \qquad (4)$$

In order to find values for $I^{\delta t}_{J_f}$, we took a double resonance spectrum at δt = 15-50 ns; to find values for $I^{eq}_{J_f}$ we took a spectrum at delay times long enough for the CO to achieve rotational equilibrium, 1.5 - 2 μs. **Figure 2(b)** shows a double resonance spectrum in rotational equilibrium at room temperature (293 K), and **Figure 2(a)** shows a spectrum taken only 30 ns after the IR pulse, in which the majority of the population is still in J_i = 4. Since we need the intensities of the small peaks (J_f = 0—3, 5—10), we used a scale in which the J_i = 4 peaks were completely

saturated. Peaks were assigned experimentally, by taking spectra 15 ns after the IR pulse; at these time scales the population is almost entirely in the initial rotational state J_i, determined by the wavelength of the IR light. We fit all peaks to Gaussian functions with deconvolution fitting using PeakFit (SyStat) software, and the amplitudes of each peak were used to calculate the state-to-state rate constants according to the above equation.

2.2. Scattering Calculations

We used the three-dimensional Ar-CO potential energy surface recently developed by Sumiyoshi and Endo [20]. They first obtained an analytical model of the PES using 46 parameters from a set of 2448 ab-initio points calculated at the CCSD(T)-F12b/aug-cc-pV5Z level of theory. The bond length of the CO monomer covers the [1,1.35] Å interval in steps of 0.05, which enables an accurate description of the first 15 vibrational levels of CO. They then used these parameters as initial values for the least-squares analysis of the available experimental spectroscopic data including the rovibrational spectrum of the complex. A total of 20 parameters were optimized to reproduce all the spectroscopic data. The resulting minimum D_e = 107.1 cm^{-1}, is obtained for a bent geometry at $\theta = 95°$ which is 0.9 cm^{-1} shallower than the *ab initio* value and reproduces the experimental data very well.

The rovibrationally inelastic cross-sections were calculated at the close coupling level using the Newmat package [41], which we recently used in the study of the inelastic collisions of He with vibrating NO^+ [42]. This code solves the close coupling equations in the space-fixed frame using a log derivative propagator. The vibration of the diatomic molecule is treated by first solving the exact diatomic equations using the diatomic potential and a finite basis representation of imaginary exponential as described by Colbert and Miller [43]. The diatomic rovibrational wave functions are then evaluated along a Gauss–Hermite grid and used to calculate the vibrational part of the intermolecular potential matrix elements. The inclusion of 21 rotational states for each of the three vibrational levels was sufficient to converge the cross sections in the [10^{-1}, 2000] cm^{-1} collision energy interval of our calculations. The intermolecular coordinate propagation step size was taken to be 0.015 a_0 and the maximum distance of propagation was 50 a_0 at the lowest collision energy considered in the calculations. The relative convergence criterion of the inelastic cross sections as a function of the total angular momentum was taken to be 0.1% for the whole range of energy and the maximum value of the total angular momentum needed to reach convergence was equal to 56. We estimate the global accuracy of our calculation to range between 1 and 5%.

The state-to-state rate constants $k_{vJ\to v'J'}(T)$ at temperature T were then computed by Boltzmann averaging the corresponding inelastic cross sections $\sigma_{vJ\to v'J'}(E_{vJ})$ over the collision energy E_{vJ} in the channel vJ where vJ and $v'J'$ respectively designate the vibrational and rotational quantum number of CO before and after collision.

$$k_{vJ\to v'J'}(T)=\sqrt{\frac{8}{\pi\mu}}\left(k_BT\right)^{-\frac{3}{2}}\int_0^\infty dE_{vJ}\sigma_{vJ\to v'J'}\left(E_{vJ}\right)e^{-\frac{E_{vJ}}{k_BT}} \quad (5)$$

In the following, we will also make use of the rotational $k_{vJ}^{rotquen}(T)$ and vibrational $k_{vj}^{vibquen}(T)$ quenching rate constants which are defined as follows. The rotational quenching of the rotational level j inside the vibrational level v is:

$$k_{vJ}^{rotquen}(T)=\sum_{J'<J}k_{vJ\to vJ'}(T) \quad (6)$$

while the vibrational quenching rate constant of the rovibrational level vJ is defined by

$$k_{vJ}^{vibquen}(T)=\sum_{v'<v,J'}k_{vJ\to v'J'}(T) \quad (7)$$

3. Results

3.1. Scattering Calculations

A number of state-to-state ($v = 2, J_i \rightarrow v = 2, J_f$) rotational cross sections of CO ($v = 2$) in collision with Ar are presented as a function of collision energy in **Figure 3**. Typical shape and Feshbach resonances supported by the van der Waals well can be seen for collision energies lower than the van der Waals well depth while at higher energy the cross sections increase again as a function of collision energy.

An important issue in such studies is to know whether the state-to-state mechanism for rotational relaxation within different vibrational levels (*i.e.* without vibrational relaxation) is identical, or at least nearly so (see for example Islam *et al.* [44] and Denis-Alpizar and Stoecklin [42]). This assumption relies on the fact that van der Waals wells are usually quite shallow and small compared to the diatomic vibrational spacing. In other words the intermolecular potential is not strong enough to couple different vibrational levels. Consequently vibrational quenching is negligible compared to rotational quenching for most neutral van der Waals complexes. This is indeed the case of Ar-CO as can be seen in **Figure 4** which shows the rotational and vibrational quenching rate constants from the second excited vibrational state of CO in the rotational states $J = 0$, 1, 4 and 6. The vibrational quenching rate constants are 6 to 8 orders of magnitude smaller than the rotational quenching rate constants. Consequently, the Ar-CO ($v, J_i = 6 \rightarrow v' = v, J_f$) state-to-state rotational de-excitation rate constants represented in Figure 5 for three temperatures and for the two vibrational levels $v = 1$ (left panel) and $v = 2$ (right panel) of CO are very similar. These results demonstrate that for Ar-CO the state-to-state mechanism for rotational relaxation within different vibrational levels is identical.

3.2. Experimental measurements

Experimental state-to-state rate constants and total relaxation cross sections were determined at four different temperatures (30.5, 52, 111, and 293 K) and four different values of J_i (0, 1, 4 and 6). These experimental results are compared to the theoretical rates in Tables S1—S4 for 293, 110.6, 52.2, and 30.5 K, respectively. The experimental values are given with 2σ errors, and the theoretical values are given in parentheses. In general, we find very good agreement between theory and experiment, as shown in Figure 6 which plots the state-to-state rate constants for theory and experiment for 110.6 K and J_i = 0, 1, 4, and 6. Tables S1—S4 compare the total removal rate constants found from fitting the first-order decay of the double resonance signal of J_i and the sum of the state-to-state rate constants. In almost all cases, these values are the same within the combined error limits, which means not only that the total removal and state-to-state experiments are consistent, but also that the state-to-state rate constants include all the major rate pathways (i.e. there are no significant contributions from J_f > 10). At room temperature, the sums of the state-to-state rate constants are generally somewhat lower than the total removal rate constants, probably due to non-inclusion of all the pathways and problems of spectral overlap. In contrast to the previous work of Carty et al [18], we did not correct or normalize these state-to-state rate constants.

Figure 7 shows a plot of the total removal cross-section with the sum of the theoretical state-to-state rate constants for J_f = 0—20. As with the state-to-state rate constants, most experimental values are within error of the theoretical values. For J_i = 1, 4, and 6 the total removal cross section increases with decreasing temperature, with larger increases for J_i = 4 and 6 than for J_i = 1. While the total removal cross-section for J_i = 0 initially increases as the temperature drops, it begins to decrease below 111 K.

4. Discussion

The temperature dependent rate constants and cross sections for collisional RET between Ar and CO can be explained by a few factors. The first is the strength of the polarizability and long-range forces of the gases. According to Sumiyoshi and Endo the CO-Ar van der Waals well is deep: 107.1 cm^{-1} or 154 K [20]. As the average collision energy decreases to below this level, we would expect Ar and CO molecules to spend more time in the van der Waals complex, leading to more efficient inelastic collisions and higher cross sections. As the temperature of the gas decreases, we would also expect to see a reduction in cross sections for endothermic pathways, which rely on collisional excitation of CO molecules to overcome the endothermicity of the reaction. The number of available exothermic pathways is different for different J values; J = 0 has none ($\Delta J > 0$ for all transitions) whereas J = 6 has six exothermic pathways (J_f = 0, 1, 2, 3, 4, and 5).

4.1 Total Removal Cross-Sections

The measured total removal cross-sections (Figure 7) were large compared to those of lighter rare gases. Carty *et al*. [18] report a total removal cross-section from $J_i = 1$ at ambient temperature of (22.3 ± 0.6) Å^2 for the rotational relaxation of CO in He, and Hostutler *et al*. [45] report a total removal cross section of 29.2 Å^2 for the rotational relaxation of CO in Ne. Both these values are significantly lower than the value of 65.0 ± 5.7 Å^2 for CO in Ar. For every temperature the cross sections from Carty *et al*. taken in a He bath gas are 2 - 3 times smaller than those reported here with an Ar bath gas. This trend follows the relative magnitudes of the CO-He, CO-Ne and CO-Ar van der Waals wells, which are calculated to be 22.34 cm^{-1} [46], 49.4 cm^{-1} [47], 107.1 cm^{-1} [20] respectively. A deeper van der Waals well increases the strength of the interaction between CO and the noble gas and the likelihood of inelastic collisions. This trend agrees with long known trends for collisional broadening; the heavier rare gases with stronger polarizability and deeper van der Waals wells lead to greater collisional broadening [10].

While the absolute cross sections were bigger for CO RET in Ar than compared to He, the general trends of the total cross sections with temperature are very similar to those found by Carty *et al*. [18] for CO-He. For the larger values of J_i, (here, $J_i = 4$ and 6) there are many exothermic pathways available, and the total removal cross sections increase as the temperature drops due to the influence of the van der Waals well. The temperature dependence is more complicated for $J_i = 0$ and 1, which have no or only one exothermic ($\Delta J < 0$) pathways available. While long range forces still play a significant role at lower temperatures, this is offset by the decreased energy of the Ar bath gas which disfavors endothermic reactions. Carty *et al*. [18] found that the temperature dependence of the total removal cross section of $J_i = 1$ was essentially temperature independent with these two effects essentially counteracting each other, and we obtain a similar result, though we see a small (and probably insignificant) increase of the cross section for $J_i = 1$ at the lowest temperature. Like Carty *et al.,* we also saw a noticeable decrease in the cross section at lower temperatures for $J_i = 0$ [18]. This is expected given that there are no exothermic channels available.

4.2 State-to-State Rate Constants

Again, we see many trends in the state-to-state rate constants that are similar to those found by Carty *et al* [18]. Firstly, rate constants are largest when J_f is close to J_i (ΔJ is small), and decrease as ΔJ increases. This is explained by the larger collision energy needed to transfer the greater amounts of energy for high ΔJ transitions. We also observe narrower distributions of the state-to-state rate constants as the temperature decreases, because in a lower temperature bath gas the lower average collision energy will disfavor transitions that require large energy transfers. This effect favors low ΔJ transitions and narrows the distribution of state-to-state rate constants.

Finally, we do see a slight propensity for ΔJ = odd transitions, most clearly seen in the data for $J_i = 0$ at room temperature, since at lower temperatures this effect is washed out by the

steep decrease in rate as ΔJ increases. As previously described by McCurdy and Miller [48], this effect arises from resonances, and is a purely quantum effect. It can be understood more intuitively by looking in Figure S8 at the variation of the expansion coefficients of the PES in Legendre polynomials as a function of the intermolecular distance. While the magnitudes of the even coefficients are larger than those of the odd coefficients, it can be also clearly seen that the odd values of l are associated with attractive contribution while the even coefficients are repulsive. These simple facts explain the observed and calculated propensity rule for this system. A similar behavior was also observed in the CO – He system by Carty et al. [18].

4.3 Comparison of experimental and theoretical results

The agreement between the experimental and theoretical results is excellent. In contrast to many other experimental methods, here there is no scaling factor applied and absolute rate constants / cross-sections are obtained. At the state-to-state level essentially quantitative agreement is obtained within the error limits of the experimental results, as can be seen for example in Figure 6 at 111 K. The total cross sections for relaxation of specific states also show very good agreement, especially for J_i = 4, 6 (see Figure 7) where quantitative agreement is obtained. The experimental results for J_i = 0 appear to drop somewhat more than theory predicts at the lowest temperatures and for J_i = 1 appear slightly lower than the theoretical predictions. It is possible that these slight differences, especially at very low temperatures, can be traced to small differences in the long-range anisotropic part of the potential of Sumiyoshi and Endo [20] which was refined by comparison with spectroscopic data arising from bound states of the Ar-CO complex. However, the main point that should be emphasized here is the remarkable and essentially quantitative agreement between experiment and theory.

5. Conclusions

Absolute state-to-state and total relaxation rate constants/cross-sections have been measured for rotational energy transfer in collisions between CO (v = 2, J_i) and Ar over the temperature range 30.5—293 K for J_i = 0, 1, 4, 6 using an infrared – vacuum ultraviolet double resonance technique. Rovibrationally inelastic rate constants/cross-sections have been calculated at the close coupling level on the newly available potential of Sumiyoshi and Endo [20]. The rotational relaxation rate constants were shown to be insensitive to vibrational state of CO, and excellent agreement was found between the theoretical predictions and the experimental measurements, emphasizing the high quality of the potential.

Acknowledgements

The authors acknowledge financial support from the French *Agence Nationale de la Recherche* (ANR-HYDRIDES, contract ANR-12-BS05-0011-01). LM thanks Rennes Metropole for a mobility grant, and the Office for Science and Technology of the Embassy of France in the United States for a Chateaubriand Fellowship.

Figures

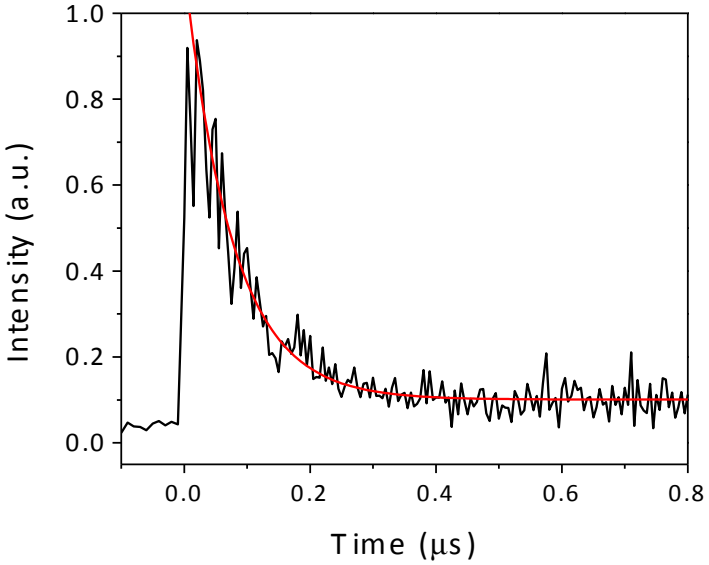

Figure 1 A typical LIF decay (black) used to find total removal rate constants, taken at 52 K with $J_i = 0$ (IR wavelength = 2349.5 nm) and detecting the LIF signal of the Q(0) branch in the excited state at 165.317 nm) with a 5 ns step size. The exponential fit is shown in red.

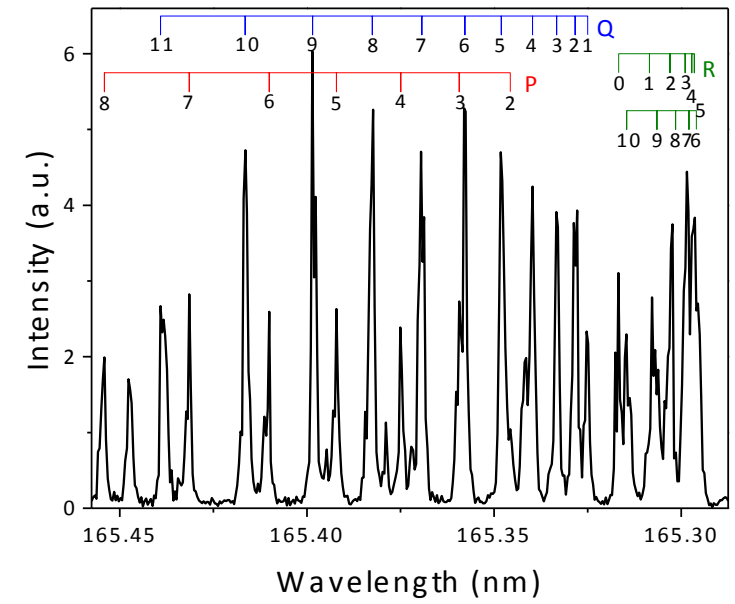

(a)

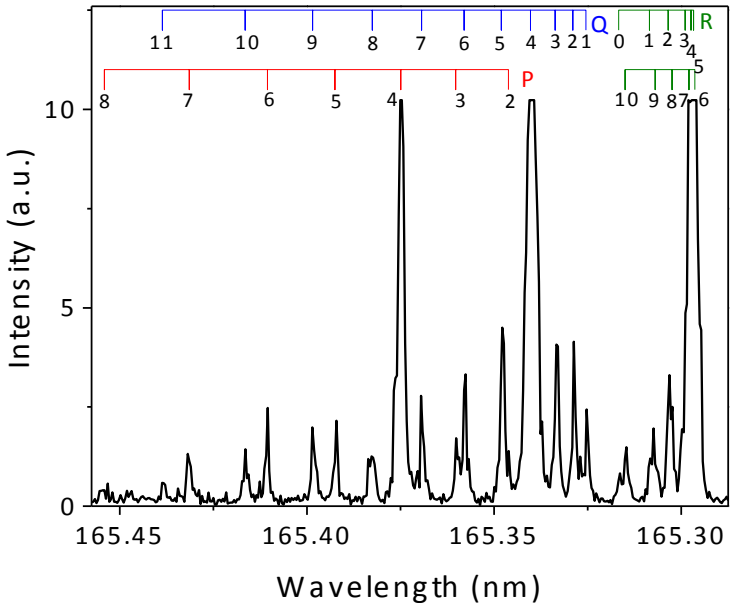

(b)

Figure 2 Double resonance spectra taken at room temperature at a (a) 1.5 μs delay, in which the CO is in rotational equilibrium and (b) 30 ns delay, in which most of the population is still in the initially excited rotational level, $J_i = 4$ in this case.

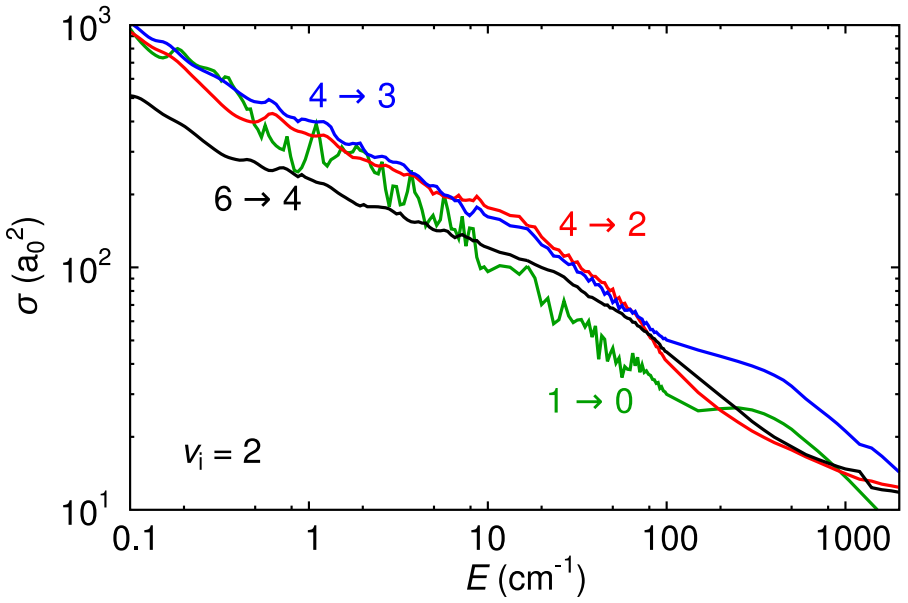

Figure 3 Variation as a function of collision energy of a few state-to-state ($v = 2, J_i \rightarrow v' = 2, J_f$) calculated rotational energy transfer cross-sections for CO in collision with Ar.

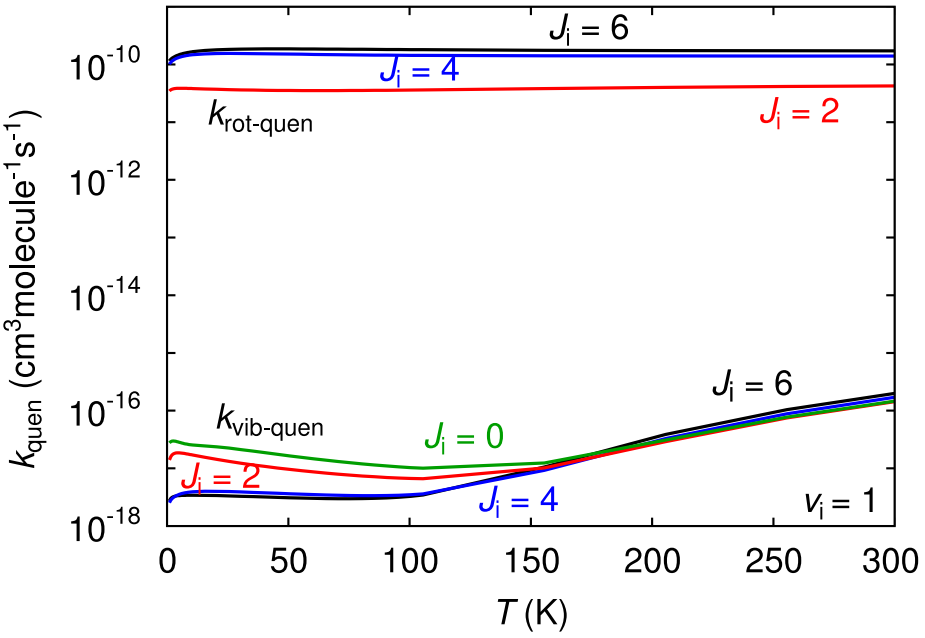

Figure 4 Rotational and vibrational quenching rate constants of CO in collision with Ar.

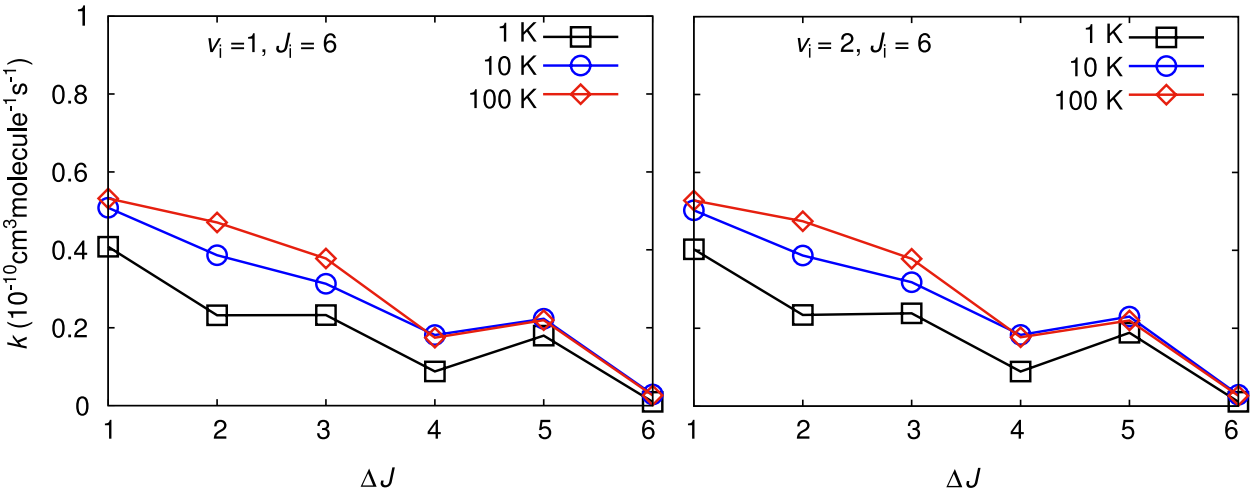

Figure 5 Comparison of the rotational de-excitation rate constants of CO from J_i = 6 in collisions with Ar inside the vibrational level v = 1 (left panel) and v = 2 (right panel) at 1 K, 10 K and 100 K.

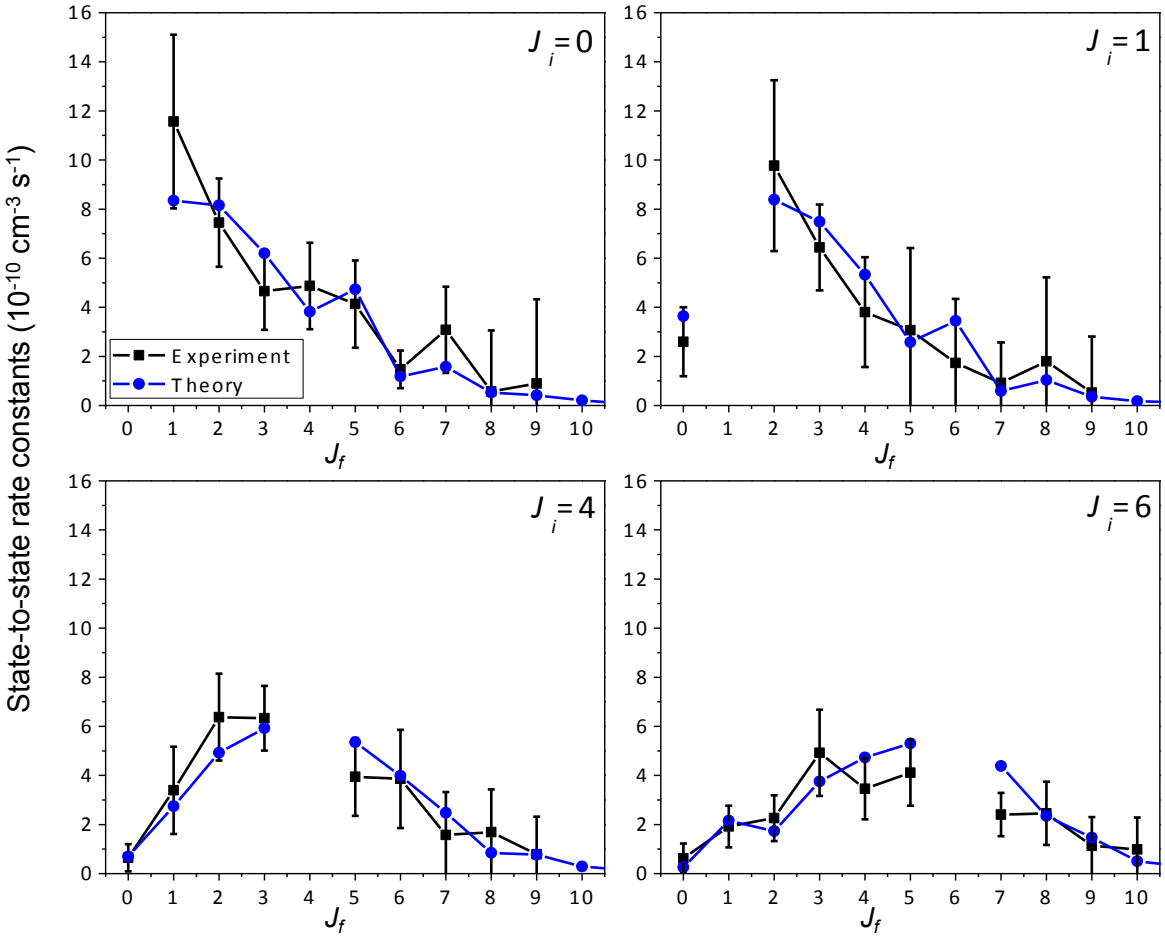

Figure 6 Experimental state-to-state rate constants for J_i =0, 1, 4,and 6 at 111 K (black filled squares, 2σ error) compared to theoretical state-to-state rate constants (blue filled circles).

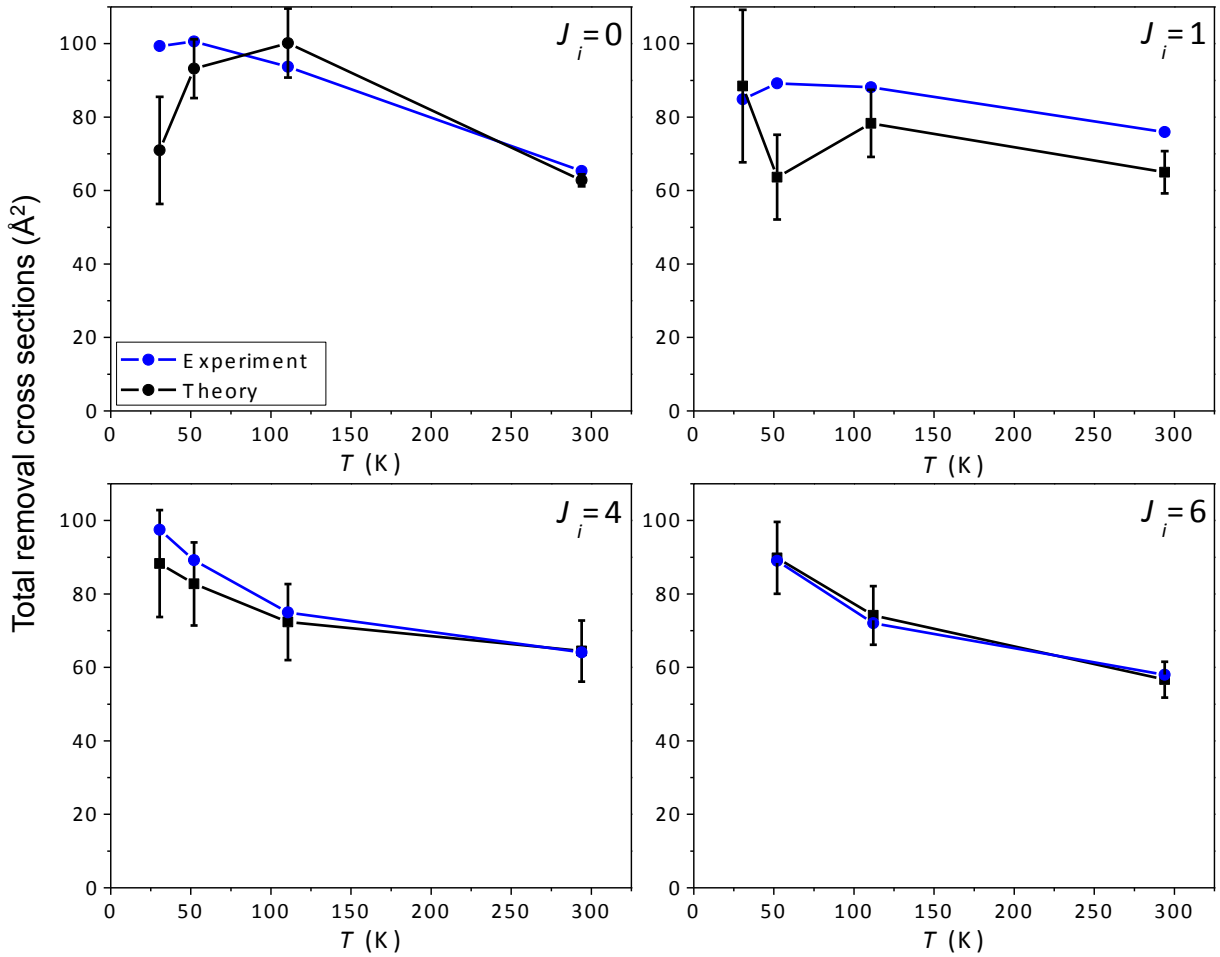

Figure 7 Experimental total experimental removal cross-sections (Å^2) for J_i = 0, 1, 4 and 6 at T = 295, 111, 52, and 30.5 K (black filled squares, 2σ error) compared to the total theoretical cross sections, found by summing the theoretical state-to-state rate constants for J_f = 0-20 (blue filled circles).

References

[1] M Havenith, GW Schwaab, Attacking a small beast: Ar-CO, a prototype for intermolecular forces, Z. Phys. Chem. 219 (2005) 1053-88.

[2] AK Dham, SC Gupta, EMPIRICAL RELATION FOR HIGHER-ORDER CONTRIBUTIONS TO VISCOSITY OF BINARY GAS-MIXTURES, J. Phys. B: At., Mol. Opt. Phys. 9 (1976) L127-L30.

[3] AK Dham, GC McBane, FRW McCourt, WJ Meath, An exchange-Coulomb model potential energy surface for the Ne–CO interaction. II. Molecular beam scattering and bulk gas phenomena in Ne–CO mixtures, J. Chem. Phys. 132 (2010) 024308.

[4] AK Dham, FRW McCourt, WJ Meath, An exchange-Coulomb model potential energy surface for the Ne-CO interaction. I. Calculation of Ne-CO van der Waals spectra, J. Chem. Phys. 130 (2009) 244310.

[5] AS Dickinson, MS Lee, CLASSICAL TRAJECTORY CALCULATIONS OF DIFFUSION AND VISCOSITY FOR HE-N2 MIXTURES, J. Phys. B: At., Mol. Opt. Phys. 18 (1985) 4177-84.

[6] EL Heck, AS Dickinson, TRADITIONAL TRANSPORT-PROPERTIES OF CO, Physica A 217 (1995) 107-23.

[7] R Moszynski, T Korona, PES Wormer, A Vanderavoird, AB-INITIO POTENTIAL-ENERGY SURFACE, INFRARED-SPECTRUM, AND 2ND VIRIAL-COEFFICIENT OF THE HE-CO COMPLEX, J. Chem. Phys. 103 (1995) 321-32.

[8] FRW McCourt, MA ter Horst, EL Heck, AS Dickinson, Transport properties of He-CO mixtures, Mol. Phys. 100 (2002) 3893-906.

[9] FRW McCourt, D Weir, GB Clark, M Thachuk, Transport and relaxation properties of isotopomeric hydrogen-helium binary mixtures. I. H-2-He mixtures, Mol. Phys. 103 (2005) 17-36.

[10] RB Nerf, MA Sonnenberg, PRESSURE BROADENING OF J=1 -0 TRANSITION OF CARBON-MONOXIDE, J. Mol. Spectrosc. 58 (1975) 474-78.

[11] F Thibault, B Calil, J Buldyreva, M Chrysos, JM Hartmann, JP Bouanich, Experimental and theoretical CO2-Ar pressure-broadening cross sections and their temperature dependence, Phys. Chem. Chem. Phys. 3 (2001) 3924-33.

[12] F Thibault, RZ Martinez, JL Domenech, D Bermejo, JP Bouanich, Raman and infrared linewidths of CO in Ar, J. Chem. Phys. 117 (2002) 2523-31.

[13] DC Clary, TS Stoecklin, AG Wickham, RATE CONSTANTS FOR CHEMICAL-REACTIONS OF RADICALS AT LOW-TEMPERATURES, J. Chem. Soc., Faraday Trans. 89 (1993) 2185-91.

[14] Y Georgievskii, SJ Klippenstein, Long-range transition state theory, J. Chem. Phys. 122 (2005) 194103 17.

[15] H Guo, Quantum dynamics of complex-forming bimolecular reactions, Int. Rev. Phys. Chem. 31 (2012) 1-68.

[16] IR Sims, IWM Smith, GAS-PHASE REACTIONS AND ENERGY-TRANSFER AT VERY-LOW TEMPERATURES, Annu. Rev. Phys. Chem. 46 (1995) 109-37.

[17] DU Andrews, BR Heazlewood, AT Maccarone, T Conroy, RJ Payne, MJT Jordan, SH Kable, Photo-Tautomerization of Acetaldehyde to Vinyl Alcohol: A Potential Route to Tropospheric Acids, Science 337 (2012) 1203-06.

[18] D Carty, A Goddard, IR Sims, IWM Smith, Rotational energy transfer in collisions between CO(X 1Σ+,v=2,J=0, 1, 4, and 6) and He at temperatures from 294 to 15 K, J. Chem. Phys. 121 (2004) 4671-83.

[19] E Roueff, F Lique, Molecular Excitation in the Interstellar Medium: Recent Advances in Collisional, Radiative, and Chemical Processes, Chem. Rev. 113 (2013) 8906-38.

[20] Y Sumiyoshi, Y Endo, Three-dimensional potential energy surface of Ar-CO, J. Chem. Phys. 142 (2015) 024314.
[21] MC Salazar, JL Paz, AJ Hernandez, Test study on the excitation spectrum of the CO center dot center dot center dot Ar van der Waals molecule, Mol. Simul. 29 (2003) 413-16.
[22] TB Pedersen, JL Cacheiro, B Fernandez, H Koch, Rovibrational structure of the Ar-CO complex based on a novel three-dimensional ab initio potential, J. Chem. Phys. 117 (2002) 6562-72.
[23] FA Gianturco, F Paesani, The rovibrational structure of the Ar-CO complex from a model interaction potential, J. Chem. Phys. 115 (2001) 249-56.
[24] RR Toczylowski, SM Cybulski, An ab initio study of the potential energy surface and spectrum of Ar-CO, J. Chem. Phys. 112 (2000) 4604-12.
[25] R Wehr, A Vitcu, F Thibault, JR Drummond, AD May, Collisional line shifting and broadening in the fundamental P-branch of CO in Ar between 214 and 324 K, J. Mol. Spectrosc. 235 (2006) 69-76.
[26] LH Coudert, I Pak, L Surin, The potential energy surface of the Ar-CO complex obtained using high-resolution data, J. Chem. Phys. 121 (2004) 4691-98.
[27] I Scheele, M Havenith, High-resolution IR spectroscopy of a high lying K-a=0 mode of the weakly bound van der Waals complex Ar-CO, Mol. Phys. 101 (2003) 1423-27.
[28] DG Melnik, S Gopalakrishnan, TA Miller, FC De Lucia, S Belov, Submillimeter wave vibration-rotation spectroscopy of Ar center dot CO and Ar center dot ND3, J. Chem. Phys. 114 (2001) 6100-06.
[29] ARW McKellar, Infrared spectrum of the Ar-CO complex: observation of the (v)co=2 <- 0 band at 4260 cm (-1), Mol. Phys. 98 (2000) 111-15.
[30] M Hepp, R Gendriesch, I Pak, YA Kuritsyn, F Lewen, G Winnewisser, M Brookes, ARW McKellar, JKG Watson, T Amano, Millimetre-wave spectrum of the Ar-CO complex: the K=2<-1 and 3<-2 subbands, Mol. Phys. 92 (1997) 229-36.
[31] SS Dimov, CR Vidal, ROTATIONAL COLLISION CROSS-SECTIONS OF THE SYSTEM CO A1-PI-M (M=HE, AR, H2) FROM A 2-STEP EXCITATION, Chem. Phys. 164 (1992) 107-14.
[32] EJ Kruus, IR ABSORPTION IN CROSSED JETS - RELATIVE ROTATIONAL ENERGY-TRANSFER EFFICIENCIES FOR CO(J=0,1) WITH HE, N2, AND AR, J. Phys. Chem. 98 (1994) 3099-107.
[33] AE Belikov, MA Smith, State-to-state rate coefficients for rotational relaxation of CO in Ar, J. Chem. Phys. 110 (1999) 8513-24.
[34] BR Rowe, G Dupeyrat, JB Marquette, P Gaucherel, STUDY OF THE REACTIONS N-2+ + 2N2- N-4+ + N2 AND O-2+ + 2O2- O-4+ + O2 FROM 20 TO 160 K BY THE CRESU TECHNIQUE, J. Chem. Phys. 80 (1984) 4915-21.
[35] G Dupeyrat, JB Marquette, BR Rowe, Design and Testing of Axisymmetric Nozzles for Ion-Molecule Reaction Studies Between 20-Degrees K and 160-Degrees K, Phys. Fluids 28 (1985) 1273-79.
[36] IR Sims, JL Queffelec, A Defrance, C Rebrionrowe, D Travers, P Bocherel, BR Rowe, IWM Smith, ULTRALOW TEMPERATURE KINETICS OF NEUTRAL-NEUTRAL REACTIONS - THE TECHNIQUE AND RESULTS FOR THE REACTIONS CN+O-2 DOWN TO 13 K AND CN+NH3 DOWN TO 25 K, J. Chem. Phys. 100 (1994) 4229-41.
[37] PL James, IR Sims, IWM Smith, Total and state-to-state rate coefficients for rotational energy transfer in collisions between NO($X^2\Pi$) and He at temperatures down to 15 K, Chem. Phys. Lett. 272 (1997) 412-18.
[38] PL James, IR Sims, IWM Smith, Rate coefficients for the vibrational self-relaxation of NO($X^2\Pi$, v = 3) at temperatures down to 7 K, Chem. Phys. Lett. 276 (1997) 423-29.

[39] PL James, IR Sims, IWM Smith, MH Alexander, MB Yang, A combined experimental and theoretical study of rotational energy transfer in collisions between NO(X (2)Pi(1/2), v=3,J) and He, Ar and N-2 at temperatures down to 7 K, J. Chem. Phys. 109 (1998) 3882-97.
[40] R Hilbig, R Wallenstein, TUNABLE VUV RADIATION GENERATED BY 2-PHOTON RESONANT-FREQUENCY MIXING IN XENON, IEEE J. Quantum Electron. 19 (1983) 194-201.
[41] T Stoecklin, A Voronin, JC Rayez, Vibrational quenching of N-2 (nu=1, j(rot)=j) by He-3: Surface and close-coupling calculations at very low energy, Phys. Rev. A 66 (2002) 042703.
[42] O Denis-Alpizar, T Stoecklin, Rovibrational rate coefficients of NO+ in collision with He, Mon. Not. R. Astron. Soc. 451 (2015) 2986-90.
[43] DT Colbert, WH Miller, A NOVEL DISCRETE VARIABLE REPRESENTATION FOR QUANTUM-MECHANICAL REACTIVE SCATTERING VIA THE S-MATRIX KOHN METHOD, J. Chem. Phys. 96 (1992) 1982-91.
[44] M Islam, IWM Smith, JW Wiebrecht, RATE COEFFICIENTS FOR STATE-TO-STATE ROVIBRONIC RELAXATION IN COLLISIONS BETWEEN NO(X(2)II, NU=2,OMEGA,J) AND NO, HE, AND AR AT 295, 200, AND 80 K, J. Chem. Phys. 103 (1995) 9676-91.
[45] DA Hostutler, TC Smith, GD Hager, GC McBane, MC Heaven, State-to-state rotational relaxation rate constants for CO plus Ne from IR-IR double-resonance experiments: Comparing theory to experiment, J. Chem. Phys. 120 (2004) 7483-89.
[46] KA Peterson, GC McBane, A hierarchical family of three-dimensional potential energy surfaces for He-CO, J. Chem. Phys. 123 (2005) 084314.
[47] ZQ Wang, EY Feng, HJ Yu, CZ Zhang, JM Du, A new ab initio potential energy surface for the NeCO complex with the vibrational coordinate dependence, J. Chem. Phys. 134 (2011) 024320.
[48] CW McCurdy, WH Miller, Interference effects in rotational state distributions: Propensity and inverse propensity, J. Chem. Phys. 67 (1977) 463-68.

Supplementary Figures and Tables for Mertens et al.

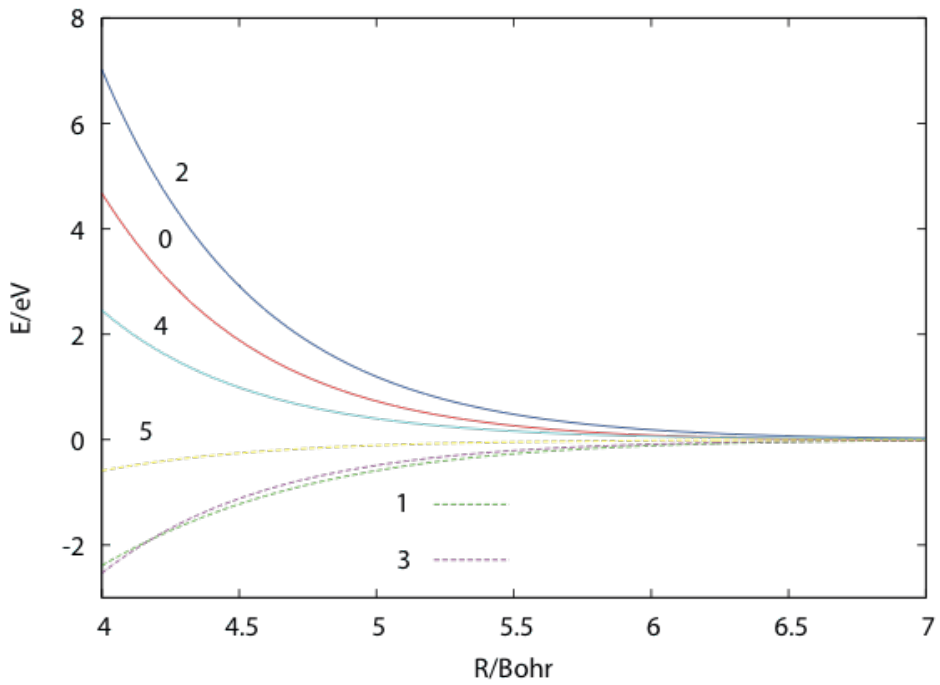

Figure S8 Legendre expansion coefficients $v_l(R)$ of the PES as a function of the intermolecular distance. The CO distance is fixed at its experimental value and the curves are labeled by the corresponding value of l.

Table S1. State-to-state rate constants for transfer between initial and final rotational states of CO in collision with Ar at ambient temperature (293 K) in units of 10^{-11} cm^{-3} s^{-1}. Experimental values are given with 2σ statistical errors and compared to theoretical values which are given in parentheses.

J_{final}	$J_{Initial}$			
	0	1	4	6
0	$J_{Initial}$	-	-	-
1	6.9 ± 1.9 (6.7)	$J_{Initial}$	1.7 ± 0.6 (2.3)	1.4 ± 0.7 (1.7)
2	3.7 ± 0.8 (7.4)	5.1 ± 0.7 (10.2)	2.0 ± 0.3 (4.4)	1.4 ± 0.5 (1.5)
3	4.8 ± 1.7 (5.6)	5.2 ± 1.0 (8.2)	4.8 ± 0.7 (6.7)	1.9 ± 0.7 (3.4)
4	2.3 ± 1.1 (4.0)	4.3 ± 1.1 (5.9)	$J_{Initial}$	4.3 ± 0.9 (4.6)
5	3.6 ± 1.7 (5.2)	3.6 ± 1.4 (3.3)	4.1 ± 0.7 (7.1)	5.7 ± 0.9 (5.9)
6	1.7 ± 1.5 (1.7)	3.4 ± 0.7 (5.1)	3.8 ± 0.9 (5.4)	J_{Initia}
7	3.9 ± 1.9 (3.4)	1.3 ± 0.9 (1.5)	3.0 ± 0.7 (4.1)	4.0 ± 0.8 (5.7)
8	1.4 ± 1.4 (1.2)	2.5 ± 0.9 (3.1)	1.4 ± 0.7 (2.0)	3.8 ± 0.9 (4.0)
9	1.4 ± 1.4 (1.8)	1.0 ± 0.9 (1.2)	1.6 ± 0.5 (2.5)	3.0 ± 0.9 (3.1)
10	0.9 ± 1.4 (0.9)	0.9 ± 0.7 (1.3)	1.0 ± 0.5 (1.1)	1.6 ± 0.6 (1.5)
$\Sigma k_{st\text{-}to\text{-}st}$	30.7 ± 4.8 (37.9)	27.3 ± 2.8 (39.8)	23.4 ± 1.9 (35.6)	27.1 ± 2.3 (31.3)
k_{Total}	38.6 ± 1.0 (40.2)	40.0 ± 3.5 (46.7)	39.8 ± 2.7 (39.4)	34.8 ± 3.0 (35.6)

Table S2. State-to-state rate constants for transfer between initial and final rotational states of CO in collision with Ar at 111 K in units of 10^{-11} cm^{-3} s^{-1}. Experimental values are given with 2σ statistical errors and compared to theoretical values which are given in parentheses.

J_{final}	$J_{Initial}$			
	0	1	4	6
0	$J_{Initial}$	2.6 ± 1.4 (3.6)	6.5 ± 0.6 (6.9)	0.6 ± 0.6 (0.3)
1	11.2 ± 3.5 (8.3)	$J_{Initial}$	3.4 ± 1.8 (2.7)	1.9 ± 0.8 (2.2)
2	7.5 ± 1.8 (8.2)	9.8 ± 3.5 (8.4)	6.4 ± 1.8 (4.9)	2.3 ± 0.9 (1.7)
3	4.7 ± 1.6 (6.2)	6.4 ± 1.8 (7.5)	6.3 ± 1.3 (5.9)	4.9 ± 1.8 (3.8)
4	4.9 ± 1.8 (3.8)	3.8 ± 2.2 (5.3)	$J_{Initial}$	3.5 ± 1.2 (4.7)
5	4.1 ± 1.8 (4.7)	3.1 ± 3.4 (2.6)	3.9 ± 1.6 (5.4)	4.1 ± 1.4 (5.3)
6	1.5 ± 0.8 (1.2)	1.7 ± 2.6 (3.4)	3.9 ± 2.0 (4.0)	$J_{Initial}$
7	3.1 ± 1.8 (1.6)	0.9 ± 1.6 (0.6)	1.6 ± 1.8 (2.5)	2.4 ± 0.9 (4.4)
8	0.6 ± 2.5 (0.5)	1.8 ± 3.4 (1.0)	1.7 ± 1.7 (0.8)	2.5 ± 1.3 (2.3)
9	0.9 ± 3.4 (0.4)	0.5 ± 2.3 (0.4)	0.8 ± 1.5 (0.8)	1.1 ± 1.2 (1.5)
10	-	-	-	1.0 ± 1.3 (0.5)
$\Sigma k_{st\text{-}to\text{-}st}$	38.7 ± 6.8 (35.0)	30.6 ± 7.7 (32.8)	28.6 ± 4.8 (27.7)	27.8 ± 3.7 (26.6)
k_{Total}	38.0 ± 3.6 (35.3)	29.7 ± 3.5 (33.2)	27.3 ± 3.9 (28.3)	25.7 ± 3.0 (27.2)

Table S3. State-to-state rate constants for transfer between initial and final rotational states of CO in collision with Ar at 52 K in units of 10^{-11} cm^{-3} s^{-1}. Experimental values are given with 2σ statistical errors and compared to theoretical values which are given in parentheses.

J_{final}	$J_{Initial}$			
	0	1	4	6
0	$J_{Initial}$	1.8 ± 1.4 (3.5)	0.5 ± 0.6 (0.8)	0.4 ± 0.3 (0.3)
1	7.5 ± 1.4 (8.8)	$J_{Initial}$	2.4 ± 1.8 (3.0)	1.8 ± 0.4 (2.4)
2	4.0 ± 1.0 (7.0)	6.1 ± 3.5 (7.1)	4.3 ± 1.8 (5.6)	2.3 ± 0.5 (2.0)
3	3.3 ± 1.3 (4.6)	3.0 ± 1.8 (6.1)	4.6 ± 1.3 (5.7)	3.7 ± 0.8 (3.8)
4	1.7 ± 1.5 (2.7)	2.8 ± 2.2 (3.5)	$J_{Initial}$	2.6 ± 0.5 (4.7)
5	1.8 ± 1.5 (2.4)	1.0 ± 3.4 (1.4)	3.3 ± 1.6 (3.9)	2.9 ± 1.1 (5.2)
6	0.5 ± 2.9 (0.4)	0.7 ± 2.6 (1.3)	1.4 ± 2.0 (2.2)	$J_{Initial}$
7	0.2 ± 2.1 (0.2)	-	0.6 ± 1.8 (0.9)	2.7 ± 1.5 (3.0)
8	-	-	-	1.3 ± 2.5 (1.0)
$\Sigma k_{st\text{-}to\text{-}st}$	18.9 ± 4.7 (26.0)	15.4 ± 2.2 (22.9)	17.1 ± 3.6 (22.0)	17.8 ± 3.3 (22.6)
k_{Total}	24.1 ± 2.3 (26.0)	18.1 ± 3.2 (23.1)	21.4 ± 2.9 (22.3)	23.2 ± 2.5 (23.1)

Table S4. State-to-state rate constants for transfer between initial and final rotational states of CO in collision with Ar at 30.5 K in units of 10^{-11} cm^{-3} s^{-1}. Experimental values are given with 2σ statistical errors and compared to theoretical values which are given in parentheses.

J_{final}	$J_{Initial}$		
	0	1	4
0	$J_{Initial}$	5.0 ± 1.2 (3.6)	0.9 ± 0.7 (1.0)
1	5.4 ± 0.7 (8.8)	$J_{Initial}$	2.4 ± 1.2 (3.0)
2	5.2 ± 1.0 (5.6)	5.2 ± 1.0 (6.1)	5.8 ± 1.5 (5.8)
3	2.5 ± 1.5 (2.9)	4.7 ± 1.2 (4.4)	4.0 ± 1.7 (5.7)
4	1.8 ± 1.3 (1.5)	2.2 ± 1.4 (1.8)	$J_{Initial}$
5	0.5 ± 1.0 (0.8)	0.5 ± 1.1 (0.6)	2.6 ± 1.5 (2.7)
6	0.3 ± 0.8 (0.1)	0.7 ± 2.0 (0.3)	1.1 ± 2.8 (0.9)
$\Sigma k_{st\text{-}to\text{-}st}$	15.6 ± 2.6 (19.7)	18.4 ± 3.3 (16.8)	16.7 ± 4.2 (19.1)
k_{Total}	14.0 ± 2.9 (19.7)	17.5 ± 4.1 (16.8)	17.5 ± 2.9 (19.3)